

IMECE2006-15111

VISION BASED FORCE SENSING FOR NANOROBOTIC MANIPULATION

Abhishek Gupta*

Volkan Patoglu

Marcia K. O'Malley

Department of Mechanical Engineering

Rice University

Houston, Texas, 77005

{abhi, vpatoglu, omalleym}@rice.edu

ABSTRACT

Over the last decade, considerable interest has been generated in building and manipulating nanoscale structures. Applications of nanomanipulation include study of nanoparticles, molecules, DNA and viruses, and bottom-up nanoassembly. We propose a Nanomanipulation System using the Zyvex S100 nanomanipulator, which operates within a scanning electron microscope (SEM), as its primary component. The primary advantage of the S100 setup over standard scanning probe microscopy based nanomanipulators is the ability to see the object during manipulation. Relying on visual feedback alone to control the nanomanipulator is not preferable due to perceptual limitations of depth and contact within the SEM. To improve operator performance over visual feedback alone, an impedance-controlled bilateral teleoperation setup is envisioned. Lack of on-board force sensors on the S100 system is the primary hindrance in the realization of the proposed architecture. In this paper, we present a computer vision based force sensing scheme. The advantages of this sensing strategy include its low cost and lack of requirement of hardware modification(s). Force sensing is implemented using an atomic force microscopy (AFM) probe attached to the S100 end-effector. Deformation of the cantilever probe is monitored using a Hough transform based algorithm. These deformations are mapped to corresponding end-effector forces following the Euler-Bernoulli beam mechanics model. The forces thus sensed can be used to provide force-feedback to the operator through a master manipulator.

NOMENCLATURE

x	in plane horizontal axis
y	in plane vertical axis
z	out of plane axis
s	distance along the beam from point \mathbf{P}_0 to \mathbf{P}_1
$\rho(s)$	curvature at s
$r(s)$	radius of curvature at s
$\phi(s)$	beam angle at s with respect to the x-axis
$M(s)$	moment at s
E	modulus of elasticity of the beam
I	moment of inertia of the beam about the z-axis
F	external transverse force at point \mathbf{P}_1
L	length of the beam
Δ	change in projected beam length
δ	vertical deflection of the beam at point \mathbf{P}_1

INTRODUCTION

Over the last decade, considerable interest has been generated in building and manipulating nanoscale structures and objects. Experiments have been conducted to interact with nanoparticles, molecules, DNA and viruses [1–4], measurement of mechanical properties of carbon nanotubes [5] and bottom-up nanoassembly [6, 7]. Nanomanipulation refers to the use of external forces for controlled positioning or assembly of nano-scale objects in 2-D or 3-D through cutting, drilling, twisting, bending, pick-and-place, push and pull kind of tasks [8]. Figure 1 depicts some basic mechanical manipulation tasks that can be

*Address all correspondence to this author.

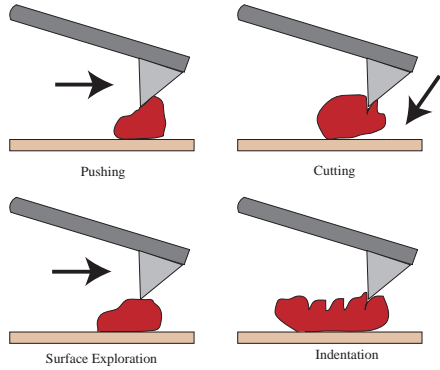


Figure 1. Possible nanomanipulation tasks using an AFM cantilever: Pushing, Cutting, Surface Exploration and Indentation. Adopted from [13].

performed at nano-scale using an AFM cantilever. Due to limitations in current understanding of nano-scale phenomenon, nanomanipulation systems are typically implemented using a telerobotic setup [9–12]. Figure 2 shows the setup of the proposed nanomanipulation system. The human operator commands a slave robot through the master robotic interface. During manipulation, the operator may be provided force or visual feedback, from the environment, or both. Visual feedback is useful for locating the objects of interest, whereas haptic feedback plays an important role in contact and depth perception.

Nanomanipulation Systems

Several research efforts have focused on development of Scanning Probe Microscopes (SPMs) for nanomanipulation systems [2, 11, 12, 14]. These systems are generally restricted to two dimensions with a very limited third dimension. Using a Scanning Tunneling Microscope (STM) probe, manipulation of atoms or molecules can be achieved by applying voltage pulses between the probe and the surface of the sample. This was first achieved by Eigler and Schweitzer in 1990 [14]. Sitti and Hashimoto [11] present the design of an AFM based telerobotic nanomanipulation system. They successfully positioned latex particles with 242- and 484-nm radii on Si substrates, with 30 nm accuracy, using an AFM cantilever as a manipulator. They adopt a two stage manipulation strategy. First, the image of the particles is obtained using AFM tapping-mode. Then the particle is pushed by moving the substrate with a constant velocity. A virtual reality interface including 3D projection display and force feedback for SPM based manipulation, known as the nanoManipulator, is presented in [2, 12]. In SPM-based nanomanipulation systems, such as these, there is no real-time visual feedback from the environment. Following their experience with the nanoManipulator, Guthold *et al.* [2] report, “Force feedback has proved essential to finding the right spot to start a modification, finding the path along which to modify, and providing

	SPM-based Nanomanipulators	Nanorobotic Manipulation Systems
System Description	Modified SPM (AFM/STM) System	Robotic System Operate within SEM/TEM
Number of Probes	1	Multiple Independent Probes
Image Resolution	< 1 nm	~ 5 nm
Position Accuracy	< 1 nm	5-10 nm
Visual Feedback during Manipulation	No	Yes
Haptic Feedback during Manipulation	Yes	Some Systems
Force/Position Sensing	Yes	Some Systems
Biological Sample Manipulation	AFM-based Systems	No

Table 1. SPM vs. SEM/TEM-based nanomanipulation systems

a subtler touch than would be permitted by the standard scan-modify-scan experiment cycle.” Hence, haptic feedback is critical in these nanomanipulation systems.

As compared to the SPM-based nanomanipulation systems, Scanning Electron Microscopy (SEM) or Transmission Electron Microscopy (TEM) based systems provide real-time visual feedback from the nanoscale environment. Dong *et al.* [15] present a 16 degree of freedom (DOF) nanorobotic manipulator that operates inside a Field Emission Scanning Electron Microscope (FE-SEM). Their system supports up to four end-effectors and has a workspace of 18 mm × 18 mm × 18 mm. The relatively large workspace, multiple end-effectors, and large number of DOFs allow complex operations with such a 3-D nanorobotic manipulator. The authors report nanorobotic manipulation to be more effective in constructing complex nanostructures than self-assembly and SPM-based systems. These systems, however, are restricted to operate in vacuum.

A comparison of SPM-based systems with SEM/TEM based systems is presented in Table 1. The primary limitation of SPM based systems is their inability to image and manipulate simultaneously. Due to drift and hysteresis, the position of tip relative to the sample may change over time. Hence, during manipulation, the user relies only upon haptic feedback. SEM/TEM-based systems on the other hand, provide real-time visual feedback but present challenges in force sensing. The nanorobotic manipulation systems provide a larger workspace for operation than SPM-based systems, but cannot match the position resolution of SPMs. AFMs can also operate in liquids, making them particularly suitable for biological applications.

Force Feedback for Nanomanipulation

Haptic feedback has been reported to be critical for nanomanipulation [2]. This is especially true for SPM-based systems, where no real-time visual feedback is available during manipula-

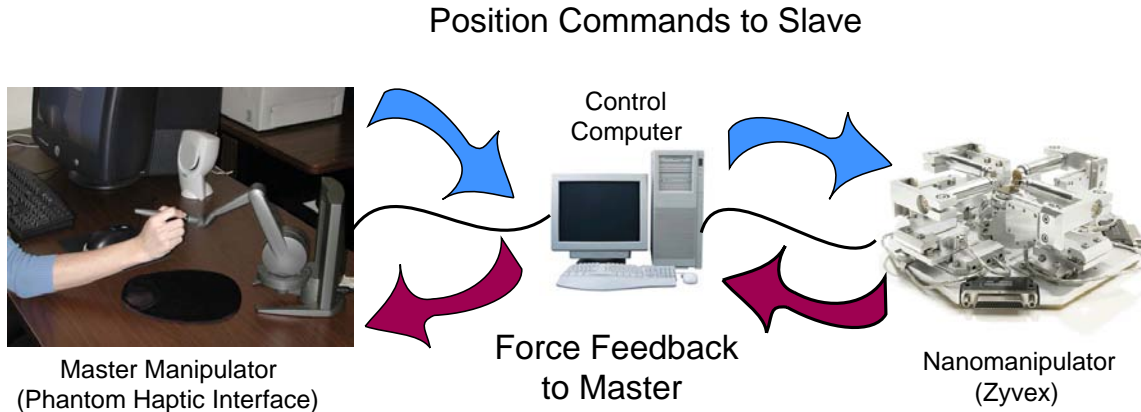


Figure 2. Typical nanomanipulation setup: A human operator commands the slave nanomanipulator. Force feedback to the operator may or may not be provided.

tion. Nanorobotic manipulators that operate inside SEM/TEMs can also benefit from incorporation of haptic feedback as it helps improve sensation of contact. Nanoscale objects could be fragile and force feedback helps the user apply controlled forces for manipulation.

Various methods of force feedback have been used for SPM-based systems. An AFM cantilever can be used as a nanoscale force sensor. Using an optical detection system, coupled normal and frictional forces can be sensed inside an AFM [9]. Piezoresistive force sensors can be incorporated into the AFM probe during fabrication to provide a compact manipulation system [10, 16]. The STM-based nanomanipulator presented by Taylor *et al.* [12] provides feedback of surface topography during manipulation using virtual springs. In later work [2], the authors report that regions of high and low friction can also be represented as high or low regions topologically.

Force sensing in nanorobotic systems that operate inside SEM/TEMs is more challenging. Arai *et al.* present a carbon nanotube based pico-Newton level force sensor [17, 18]. The nanotubes are attached to an AFM cantilever and their deformation is measured from SEM images. We are, however, not aware of any use of this information for force feedback. The range of this carbon nanotube based sensor is limited to pico-Newton levels. In addition, the nanotube may not be the ideal end-effector for general purpose nanomanipulation due to its high length-diameter ratio. Hence, there is a need for improved force sensors for such systems.

This paper presents a vision-based force sensing scheme for the proposed nanomanipulation system, which is a nanorobotic manipulation system that operates inside an SEM. An AFM cantilever is used as the end-effector and visually tracked to measure its deformation. The work is motivated from similar work by Greminger and Nelson [19], who use visual template matching

for tracking of a micro-cantilever to sense nano-newton forces at the micro level. Their approach of template matching, however, is not suitable for our application of nanomanipulation due to variable occlusion of the cantilever and loss of coherence in consecutive frames, due to the nature of implementation of the magnification functionality in the Environmental SEM (ESEM). Hence, a global search strategy is proposed that can be used for force sensing directly or to find a suitable point of initialization for subsequent template matching.

The rest of the paper is organized as follows. The following section describes the proposed nanomanipulation system following which the proposed vision-based force sensing method is discussed in detail. Thereafter, Preliminary experimental results that demonstrate the proposed force sensing algorithm, are also presented and discussed.

SYSTEM DESCRIPTION

Figure 3 depicts the overall setup of the proposed nanomanipulation system. The central component of the Rice Nano-manipulation System is the commercially available Zyvox S100 nano-manipulator (Zyvox Inc.). The S100 nanomanipulator system has a joystick based user interface that provides no haptic feedback to the user. Instead, the manipulator is designed to work inside a Scanning Electron Microscope and the user can see the object being manipulated. We have interfaced the S100 manipulator with a commercially available PHANToM haptic interface (Sensable Inc.), replacing the standard joystick. A vision-based force sensing scheme is proposed to estimate contact forces during manipulation. These sensed forces will then be scaled and reflected back to the user through the PHANToM interface. The incorporation of haptic feedback is expected to improve user perception of contact and manipulation performance.

The Zyvox S100 nanomanipulator comprises of four piezo-

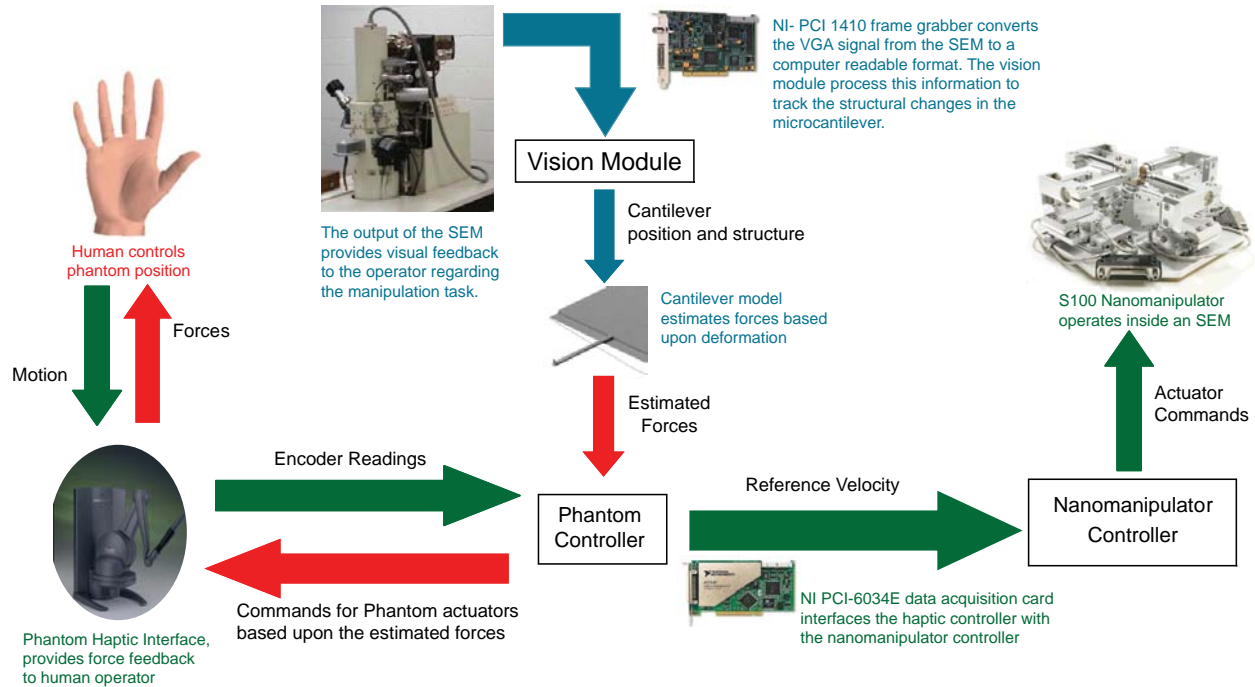


Figure 3. Overview of the proposed nanomanipulation system. The green block arrows depict the pathway for the control of the nanomanipulator. Blue block arrows correspond to force sensing subsystem, while the force feedback subsystem is shown using red block arrows. Text in black describes the information being transferred.

actuated positioners with coarse as well as fine motion stages. The motion-stages can move the positioners in a 3-D workspace of 12 mm × 12 mm × 12 mm. Detachable end-effector plugs are used to change the effectors mounted onto each positioner. This entire assembly operates under an scanning electron microscope. The ability to see the object being manipulated is a major advantage of the S100 setup over standard SPM based nanomanipulators. The presence of four end-effectors also expands the set of experiments that can be conducted with the system. The S100 is controlled using open loop rate control and can achieve up to ± 5 nm of accuracy in positioning. The primary disadvantage of the S100 system is the lack of sensory components. The SEM based imaging can provide position information at a rate of 60Hz, but the position sensing resolution is limited by image quality.

The PHANToM is used to command the nanomanipulator in a similar fashion as the original joystick, i.e, position of PHANToM end-effector is mapped to positioner velocity. A National Instruments NI-6034E Data Acquisition card is used to send PHANToM position information to the nanomanipulator controller. In order to provide a zero reference position to the operator, the PHANToM end-effector is constrained about its origin with three soft virtual springs. Any feedback from the environment is overlaid on top of these virtual springs. In order to measure forces during manipulation, an atomic force microscope (AFM) probe is mounted on the S100 positioner, as shown

in Figure 4. The output of the SEM is connected to the control computer through the PCI-1410 frame grabber from National Instruments. A vision-based scheme, as presented in the following section, is then employed to estimate contact forces.

METHODS

As described in the previous section, an AFM cantilever was mounted to the S100 positioner, as shown in Figure 4. A Hough-transform based search scheme is employed to locate the tip of the cantilever in the SEM images. The slope of the free end of

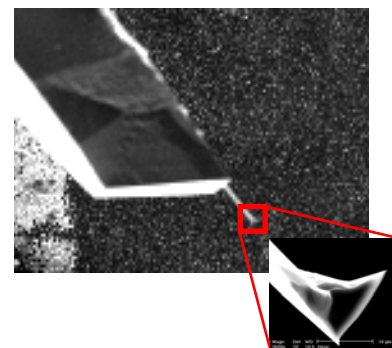


Figure 4. Attachment of the AFM cantilever probe to S100 end-effector

the cantilever is mapped to the corresponding end-point force as per the model described in the following subsection. The vision-based scheme for locating the tip of the cantilever is presented in the last subsection.

Cantilever Deformation Model

This section presents the nonlinear cantilever beam deformation model used in this work. This model is motivated by [20]. The model employs moment-curvature nonlinearity to derive a relationship between a transverse force acting on the beam and the corresponding deflection of the tip. Consider an elastic isotropic cantilever beam, fixed at \mathbf{P}_0 , with a transverse force, F , acting on the free end, \mathbf{P}_1 , as shown in Figure 5. Let s be the distance from node \mathbf{P}_0 to \mathbf{P}_1 ; $r(s)$ be the radius of curvature at s ; $\phi(s)$ be the angle of the beam at s with respect to the horizontal; ϕ_0 be the angle of beam at node \mathbf{P}_1 ; $M(s)$ be the moment at s ; E be the modulus of elasticity of the beam; I be the moment of inertial about the axis out of the plane; x and y be the in-plane horizontal and vertical axes with origin at node \mathbf{P}_0 ; L be the length of the beam; δ be the deflection at \mathbf{P}_1 ; and Δ be the projected beam shortening.

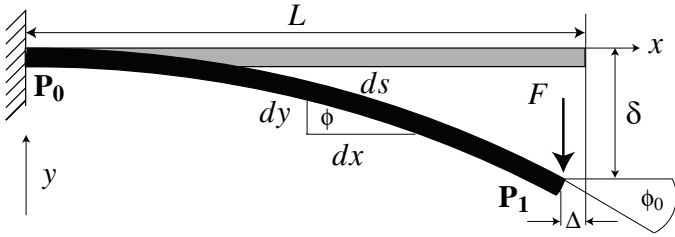


Figure 5. Cantilever Deformation Model under the Action of a Transverse Force

Then the curvature at each point, s , along the beam is given by the equation,

$$\rho(s) = \frac{1}{r(s)} = \frac{d\phi(s)}{ds} = \frac{M(s)}{EI} = -\frac{d^2y}{dx^2} \left[1 + \left(\frac{dy}{dx} \right)^2 \right]^{(-\frac{3}{2})}. \quad (1)$$

Whenever an external transverse force, F , is applied at point \mathbf{P}_1 , the curvature at s is

$$\frac{M(s)}{EI} = \frac{F(L-x-\Delta)}. \quad (2)$$

To eliminate the variable x from Equation (2), note the equality

$$\frac{dx}{ds} = \cos \phi \quad (3)$$

and differentiate Equation (2) with respect to s to derive

$$\frac{d^2\phi}{ds^2} = -\frac{F}{EI} \frac{dx}{ds} = -\frac{F}{EI} \cos \phi. \quad (4)$$

Applying the identity

$$\frac{d^2\phi}{ds^2} d\phi = \frac{1}{2} d \left(\frac{d\phi}{ds} \right)^2 \quad (5)$$

and integrating Equation (4) we have,

$$\frac{1}{2} \left(\frac{d\phi}{ds} \right)^2 = -\frac{F}{EI} \sin \phi + C \quad (6)$$

where C is the integration constant. To solve for the integration constant, C , in Equation (6), apply the following boundary conditions at point \mathbf{P}_1

$$\left. \frac{d\phi}{ds} \right|_{s=L, \phi=\phi_0} = 0 \quad (7)$$

since the moment vanishes at the free end of the beam. When the boundary conditions are applied, Equation (6) becomes

$$\frac{d\phi}{ds} = \sqrt{\frac{2F}{EI} (\sin \phi_0 - \sin \phi)} \quad (8)$$

$$\sqrt{\frac{FL^2}{EI}} = \int_0^{\phi_0} \frac{d\phi}{\sqrt{2(\sin \phi_0 - \sin \phi)}} \quad (9)$$

which gives the nondimensionalized external force at point \mathbf{P}_1 . The nondimensionalized force at point \mathbf{P}_1 can be mapped to the nondimensional traverse deflection $\delta/L = \delta(\phi_0)/L$ at \mathbf{P}_1 by equation

$$\frac{\delta}{L} = \int_0^{\phi_0} \frac{1}{\sqrt{2}} \sqrt{\frac{EI}{FL^2}} \frac{\sin \phi}{\sin \phi_0 - \sin \phi} d\phi. \quad (10)$$

Equation 9 can be integrated for different values of ϕ_0 to obtain the relationship between the external force and the slope of the cantilever at \mathbf{P}_1 . A similar relationship between the nondimensional external force and the deflection at \mathbf{P}_1 can be obtained by integrating Equation (10). The resulting plot is shown in Figure 6. These results can be used to make a lookup table to estimate forces once the angular deflection of the cantilever is estimated.

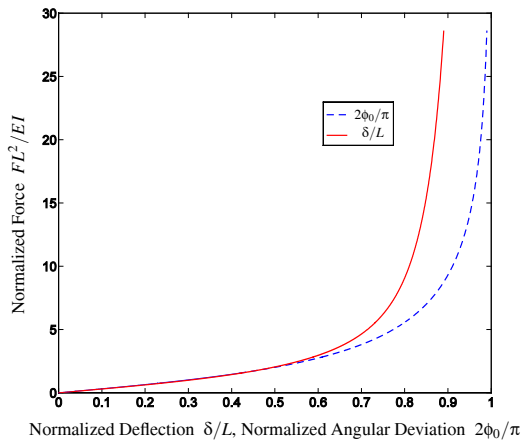


Figure 6. Nondimensional external force vs. Nondimensional angular deviation (blue, dashed) and nondimensional deflection (red, solid)

Vision-Based Force Sensing

The goal of the vision algorithm is to estimate the slope of the AFM cantilever probe, attached to the S100 positioner as shown in Figure 4, at the free end. It should be noted that the S100 system as well as the SEM provide no sensory output other than the visual output from the SEM. This coupled with the mode of operation of the SEM, which permits almost instant changes in magnification, sometimes result in loss of coherence between consecutive frames. Furthermore, with increasing magnification and decrease in the field of view, most of the cantilever is occluded. At highest magnifications, only the sharp tip of the cantilever is visible. The above-mentioned factors render the use of commonly used computer vision algorithms like template matching [19] and active contour methods [21] impractical for our implementation. These techniques usually require a good initial estimate, of the location of the feature in an image, for convergence. In order to handle the possibility of almost instant changes in the location of the cantilever tip in consecutive frames that are due to scaling effects with change in magnification settings of the microscope, we propose a Hough transform based global search scheme that effectively locates the cantilever in individual frames.

For the purpose of the proposed algorithm, the probe tip is characterized by the three edges that define the tip geometry in the image. During an initial calibration step, some pixels on the boundary of the probe tip are manually marked to estimate the initial orientation. It is assumed that the maximum deformation of the cantilever would correspond to an angular deviation of $\pm 20^\circ$, of the free end of the probe, from this initial configuration. In addition, it is assumed that the cantilever tip undergoes a pure affine transformation and no local deformation. Figure 7 depicts the algorithm for the measurement of the slope of the free end of the cantilever and subsequent contact force estimation.

Thresholding In the first step, the grey-scale image from the SEM is converted to a binary image via thresholding. The threshold is chosen experimentally based upon the average histogram of several test images. As a result of charge accumulation, the cantilever appears as one of the brightest objects in the image. Hence, this step helps remove some of the unwanted features from images.

Edge Detection The binary image obtained through thresholding is then converted to an edge image using the Canny edge operator. The Canny edge operator takes a grey-scale image as an input, and produces as output an image showing the positions of tracked intensity discontinuities. Note that only strong edge points detected by the Canny operator are selected for subsequent processing.

Line Detection The strong edge points detected by the Canny operator are provided as an input for a Hough transform-based line detection routine. The classical Hough transform is a technique to locate a parametrized feature in an image. A mesh is defined in the space of the parameters that define the feature. At each mesh point a value is accumulated. This value indicates how well the feature defined by the parameters of that mesh point fits the image. Mesh points that accumulate large values correspond to best feature match in the image. In order to detect the edges that define the tip of the cantilever probe, a slope-intercept representation of lines is used. The assumption that maximum angular deviation of the tip is restricted to $\pm 20^\circ$, helps to reduce the search space. The three edges are then individually detected in three Hough transform operations. In each step, the input point set is first transformed such that, for the initial configuration of the cantilever, the edge of interest aligns with the horizontal. The three detected lines are shown in red, blue, and green in Figure 7.

Force Mapping Once the angular deviation of the tip is estimated, the force estimate can be obtained using the lookup-table developed using the cantilever model, which is described in the previous subsection.

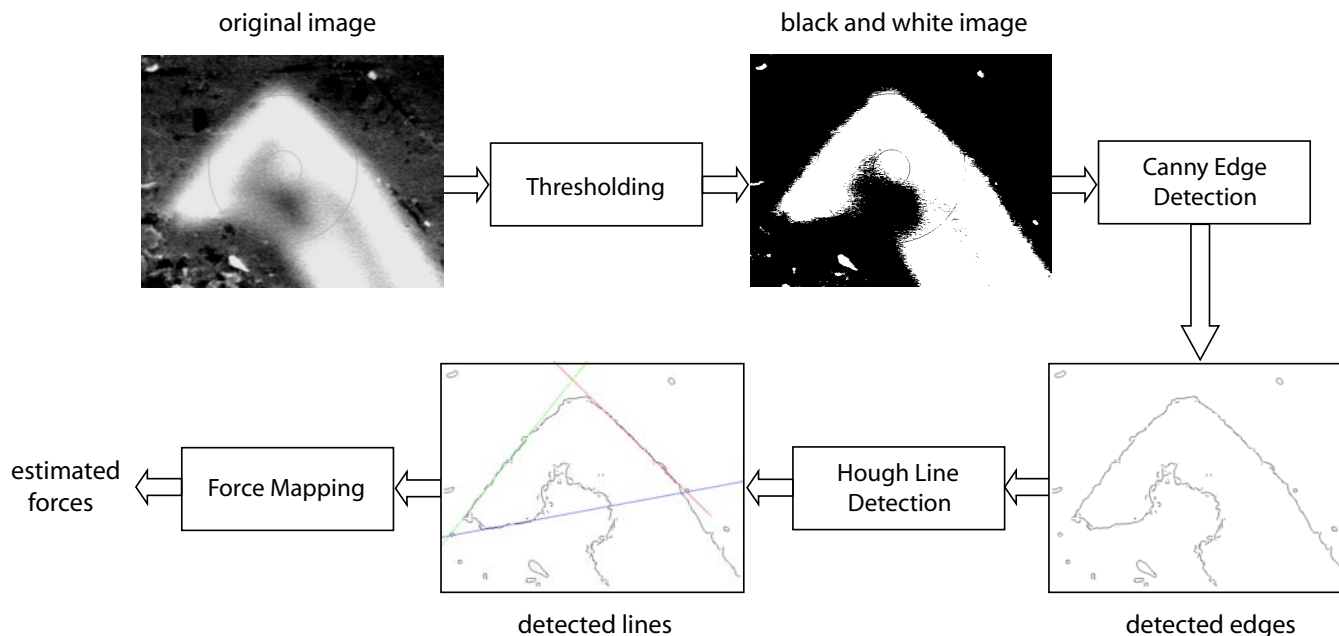


Figure 7. The Cantilever Tip Detection Algorithm

RESULTS AND DISCUSSION

For a preliminary study, the algorithm was tested upon several images of the cantilever, mounted on the S100 manipulator inside the SEM. The frames were acquired at different magnification settings for the SEM; positions of the cantilever in the field of view; and with the cantilever both above, below or in the focal plane. Individual images were rotated to test detection of the probe under rotation.

Figure 8 shows the output of the vision module as red, blue and green lines overlaid on top of the original image. Figures 8(a)– 8(c); 8(e)– 8(g) and 8(i)– 8(k) show results for rotations of 0° , 5° and 20° , at magnification levels of 3500X, 2000X and 1500X, respectively. Notice that all segments relating to the cantilever tip are successfully detected, except for 20° rotation at magnifications of 2000X and 1500X. In these two cases, the shortest segment of the tip could not be detected. Instead, the Hough transform result finds a larger value corresponding to another edge segment of the cantilever.

At low magnifications the shortest segment of the tip has fewer edge points associated with it as compared the number of edge points at some higher magnification. In addition, for large rotations some of these points may not lie on segments defined by the parametric search space, but lie just outside. These two factors will contribute to lowering of score for the line corresponding to the shortest segment with reduction in magnification of the SEM and increase in deformation of the cantilever. However, under the assumption of slow deformation of the cantilever, the algorithm can be modified by shifting the mesh, employed

for Hough transform, to the last known position of the tip segments in parameter space. Please note that unlike the position, the slope of the segments, which is used to characterize the parameter space for Hough transform implementation, is invariant under scaling. Figures 8(h) and 8(l) show the results for a rotation of 20° at magnifications of 2000X and 1500X with the mesh shifted by 15° . It can be easily verified that the algorithm now successfully finds the cantilever tip in the image.

The shortest cantilever tip segment can no longer be reliably detected using this method under a magnification of 1500X, as the length of the segment becomes comparable to size of some objects in the background and number of edge pixels associated with the tip reduce considerably. These magnification levels are not critical during nanomanipulation. Hence, the inability to detect the cantilever tip at low magnifications is not a serious drawback. At high magnification levels, when only the part of the cantilever, defined by the blue and green lines in Figure 8, is visible, the method can still be used to detect the tip orientation by identification of these two segments.

Note that force sensing with this algorithm is restricted to a single dimension. The external force is modeled as a transverse load applied at the tip of the cantilever. Unmodeled forces including frictional forces acting on the cantilever will also contribute to the deformation. Hence, the proposed vision-based sensor provides an estimate of coupled frictional and other external forces acting on the cantilever. This is, however, common in nano-scale force sensing, as decoupled estimation of force in 3-D is challenging [13].

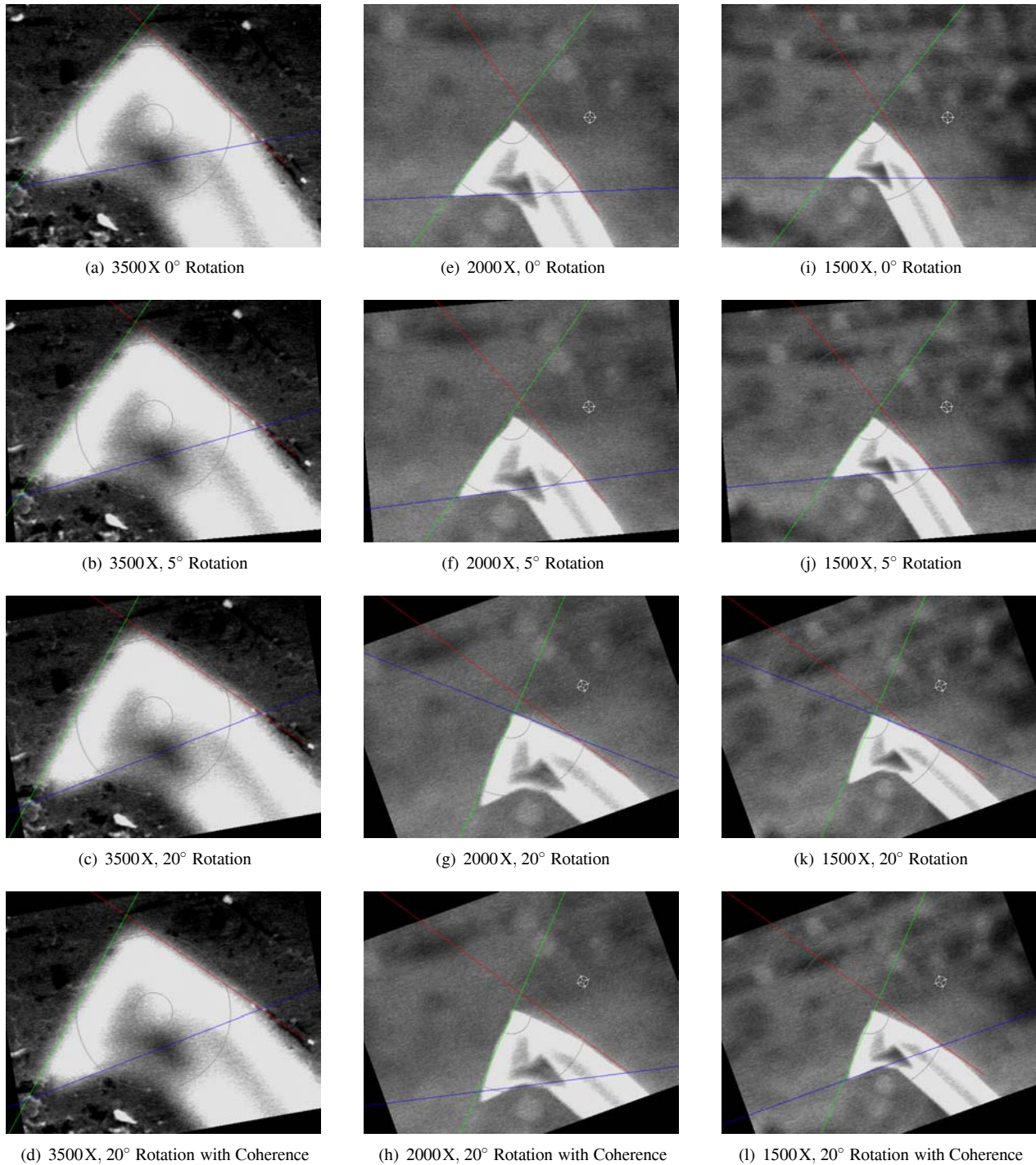


Figure 8. Performance of the vision-based sensing module. Red, blue and green Lines, overlaid on top of the original image, correspond to detected segments. Sub-figures (a)–(c); (e)–(g) and (i)–(k) show results for cantilever tip detection for rotations of 0° , 5° and 20° , at magnification levels of 3500X, 2000X and 1500X respectively. Sub-figures (d), (h) and (l) show the results, for a rotation of 20° under magnifications of 3500X, 2000X and 1500X respectively, under the assumption of slow deformation.

The accuracy and sensitivity of the force sensor presented in this article depends upon several factors. The cantilever is modeled as an isotropic, elastic beam with a uniform cross-section. In practice, real AFM cantilever probes may not be isotropic and the geometry of the tip will also affect the deformation. The limitations of the model, in addition to unmodeled forces, affect the accuracy of the sensor. Two different cantilever orientations can be distinguished if and only if they appear sufficiently distinct in images. Hence, the sensitivity of the sensor is primarily determined by the resolution of the images. When manipulating soft objects, the deflection of the cantilever may not be sufficient to be reliably detected. In such a situation, a different cantilever with lower stiffness can be employed. The image resolution and SEM magnification determine the minimum force that can be sensed by the vision-based sensor and hence the range of the sensor.

CONCLUSIONS AND FUTURE WORK

A cost-effective vision based force sensing scheme for a nanorobotic manipulation setup is presented. Preliminary experimental results indicate that the proposed methodology can be employed to successfully estimate the deformation of an AFM cantilever probe, which is used as a force sensor. Future work would involve the verification of the cantilever model with use of piezoresistive cantilevers. Calibration of the sensor would also be performed to determine the range, accuracy and sensitivity of the sensor.

ACKNOWLEDGMENT

This project was supported by the ERIT (Enriching Rice through Information Technology) program funded by the Sheafor/Lindsay Innovation Fund through the Computer and Information Technology Institute at Rice University. Zyvex Corporation donated the S100 nanomanipulator used in this work to Rice University.

REFERENCES

[1] Resch, R., Bugacov, A., Baur, C., Koel, B. E., Madhukar, A., Requicha, A. A. G., and Will, P., 1998. "Manipulation of Nanoparticles using Dynamic Force Microscopy: Simulation and Experiments". *Applied Physics A*, **67**, pp. 265–271.

[2] Guthold, M., Falvo, M. R., Matthews, W. G., Paulson, S., Washburn, S., Erie, D. A., Superfine, R., Brooks, Jr., F. P., and Taylor II, R. M., 2000. "Controlled Manipulation of Molecular Samples with the nanoManipulator". *IEEE/ASME Transactions on Mechatronics*, **5**(2).

[3] Guthold, M., Falvo, M., Matthews, W., Paulson, S., Mullin, J., Lord, S., Erie, D., Washburn, S., Superfine, R., Brooks, Jr., F. P., and Taylor II, R. M., 1999. "Identification and

Modification of Molecular Structures with the nanoManipulator". *Journal of Molecular Graphics and Modelling*, **17**, pp. 188–197.

[4] Guthold, M., Negishi, W. G. M. A., Taylor II, R. M., Erie, D., Brooks, Jr., F. P., and Superfine, R., 1999. "Quantitative Manipulation of DNA and Viruses with the nanoManipulator Scanning Force Microscope". *Surface and Interface Analysis*, **27**, pp. 437–443.

[5] Nakajima, M., Arai, F., and Fukuda, T., 2006. "In Situ Measurement of Young's Modulus of Carbon Nanotubes Inside a TEM Through a Hybrid Nanorobotic Manipulation System". *IEEE Transactions of Nanotechnology*, **5**(3), May, pp. 243–248.

[6] Requicha, A. A. G., Baur, C., Bugacov, A., Gazen, B. C., Koel, B. E., Madhukar, A., Resch, R., and Will, P., 1998. "Nano-robotic Assembly of Two-Dimensional Structures". In IEEE International Conference on Robotics and Automation.

[7] Fukuda, T., Arai, F., and Dong, L., 2003. "Assembly of Nanodevices with carbon Nanotubes Through Nanorobotic Manipulations". *Proceedings of the IEEE*, **91**(11), Nov, pp. 1803–1818.

[8] Sitti, M., and Hashimoto, H., 1999. "Teleoperated nano scale object manipulation". In *Recent Advances on Mechatronics*. Springer Verlag, pp. 322–335.

[9] Sitti, M., Aruk, B., Shintani, K., and Hashimoto, H., 2001. "Development of a Scaled Teleoperation System for Nano Scale Interaction and Manipulation". In IEEE International Conference on Robotics and Automation, pp. 850–867.

[10] Sitti, M., and Hashimoto, H., 2000. "Two-Dimensional Fine Particle Positioning Under Optical Microscope using a Piezoresistive Cantilever as Manipulator". *Journal of Microelectronics*, **1**(1), pp. 25–48.

[11] Sitti, M., and Hashimoto, H., 2000. "Controlled Pushing of Nanoparticles: Modeling and Experiments". *IEEE/ASME Transactions on Mechatronics*, **5**(2), Jun, pp. 199–211.

[12] Taylor, R. M., Robinett, W., Chi, V. L., Brooks, Jr., F. P., Wright, W. V., Williams, R. S., and Snyder, E. J., 1993. "The nanomanipulator: A virtual-reality interface for a scanning tunneling microscope". In *Computer Graphics: Proceedings of SIGGRAPH*.

[13] Sitti, M., 2001. "Survey of Nanomanipulation Systems". In IEEE Conference on Nanotechnology, pp. 75–80.

[14] Eigler, D. M., and Schweitzer, E. K., 1990. "Positioning single atoms with scanning tunneling microscope". *Nature*, **344**, Apr, pp. 524–526.

[15] Dong, L., Arai, F., and Fukuda, T., 2004. "Destructive Constructions of Nanostructures with Carbon Nanotubes Through Nanorobotic Manipulation". *IEEE/ASME Transactions on Mechatronics*, **9**(2), Jun, pp. 350–357.

[16] Tortonesi, M., Barrett, R. C., and Quate, C. F., 1993. "Atomic Resolution with an Atomic Force Microscope us-

- ing Piezoresistive Detection”. *Applied Physics Letters*, **62**, pp. 834–836.
- [17] Arai, F., Nakajima, M., Dong, L., and Fukuda, T., 2003. “Pico-Newton Order Force Measurement Using a Calibrated Carbon Nanotube Probe by Electromechanical Resonance”. In IEEE International Conference on Robotics and Automation, pp. 300–305.
- [18] Arai, F., Nakajima, M., Dong, L., and Fukuda, T., 2003. “The pico-Newton Order Force Measurement with a Calibrated Carbon Nanotube Probe”. In IEEE/ASME International Conference on Advanced Intelligent Mechatronics, pp. 691–696.
- [19] Greninger, M., and Nelson, B. J., 2004. “Vision-based force measurement”. *IEEE Transactions on Pattern Analysis and Machine Intelligence*, **26**(3), pp. 290–298.
- [20] <http://www-bsac.eecs.berkeley.edu/cadtools/-sugar/Slides/nonlinear/NLBeam.ppt>.
- [21] Xu, C., and Prince, J. L., 1998. “Snakes, Shapes and Gradient Vector Flows”. *IEEE Transactions on Image Processing*, **7**(3), pp. 359–369.